2024 IEEE/RSJ International Conference on Intelligent Robots and Systems (IROS)
October 14-18, 2024. Abu Dhabi, UAE

A Graph-Based Self-Calibration Technique for Cable-Driven Robots with Sagging Cable

M. R. Dindarloo[1], A. S. Mirjalili[1], S. A. Khalilpour[1], R. Khorrambakht[2], Stephan Weiss [3], and H. D. Taghirad[1]

***Abstract*— The efficient operation of large-scale Cable-Driven Parallel Robots (CDPRs) relies on precise calibration of kinematic parameters and the simplicity of the calibration process. This paper presents a graph-based self-calibration framework that explicitly addresses cable sag effects and facilitates the calibration procedure for large-scale CDPRs by only relying on internal sensors. A unified factor graph is proposed, incorporating a catenary cable model to capture cable sagging. The factor graph iteratively refines kinematic parameters, including anchor point locations and initial cable length, by considering jointly onboard sensor data and the robot's kineto-static model. The applicability and accuracy of the proposed technique are demonstrated through Finite Element (FE) simulations, on both large and small-scale CDPRs subjected to significant initialization perturbations.**

***Index Terms*— Cable-driven parallel robots, Kinematic calibration, Cable sag modeling, Factor graph, Self-calibration**

I. Introduction

Cables serve as a lightweight and economically viable means of transmitting energy to parallel robot moving platforms, enabling them to convey the payload from the actuator to the intended target. CDPRs use a set of cables in a parallel structure to move the object of interest in a potentially large working area. The combination of a parallel kinematic structure and lightweight cables empowers CDPRs to attain high speeds, manage substantial loads, and traverse extensive workspaces. Benefiting from these mechanical advantages, CDPRs offer promising solutions across a wide area of applications, including art [1], rescue missions [2], virtual reality [3], and operations in hazardous environments [4].

However, the challenge of using cables as a transmission link in large-scale CDPRs is the complexity caused by weight-induced sagging in the cable. This complicates the effective calibration of such platforms and impedes their widespread application. Typically, two calibration strategies are employed: utilizing the robot's internal sensors (self-calibration) or using external referencing tools such as total stations and laser range finders. While external calibration can yield high accuracy, it frequently entails time-consuming and expensive compared to self-calibration [5].

[1]M. R. Dindarloo, A. S. Mirjalili, S. A. Khalilpour, and H. D. Taghirad are with the Advanced Robotics and Automated Systems (ARAS), Faculty of Electrical Engineering, K. N. Toosi University of Technology, Tehran, Iran. taghirad@kntu.ac.ir

[2]R. Khorrambakht is with the Control/Robotics Research Laboratory, Department of Electrical and Computer Engineering, Tandon School of Engineering, New York University, Brooklyn, NY 11201 rk4342@nyu.edu

[3]Stephan Weiss is with the Department of Smart Systems Technologies, University of Klagenfurt, Austria. stephan.weiss@aau.at

This paper presents a self-calibration approach for cable robots considering the sagging effect. The novelty of this research resides in introducing a unified graph-based approach for calibrating the kinematic parameters of both large- and small-scale robots, accompanied by rigorous validation against finite element simulators to ensure accuracy. The code and implementation procedure for this approach are available on our GitHub[1].

The rest of this paper is organized as follows. Sec. II outlines related works relevant to this research emphasizing the significance of this work. Sec. III and IV elaborate on the mathematical model of the robot and our graph-based calibration pipeline. Finally, Sec. V presents the numerical studies and results, and Sec. VI provides a discussion on the solution, while the concluding remarks are given in Sec. VII.

II. Related Work

Prior research directly addressing the self-calibration of large-scale cable robots with a sagging effect is very limited. In [6], the authors introduce a self-calibration method for estimating the initial pose of a two degrees-of-freedom (DoFs) over-constrained robot with four cables. Similarly, in [7], the initial pose of a suspended underactuated CDPR is estimated using static equations. Moreover, in [8] a self-calibration method is developed using force sensors, while the authors of [9] propose a method for pose and initial length offset calibration using encoders. Following the same line, our latest work, [10], presents a graph-based self-calibration system with Monte Carlo initialization. All of these prior works consider robots with massless cables.

In terms of vision-based localization for calibration, prior works may be divided into two categories. Authors of [10], [11] place the camera on the end-effector while [12], [13] employ external cameras to localize the robot for calibration. However, it is important to note that these studies also operated under the assumption of rigid cables.

In terms of problem formulation, the kinematic calibration of CDPRs is generally written as a nonlinear least-squares (NLLS) program. Recently, factor graphs have been employed to control CDPRs using time-varying linear quadratic Gaussian control [14], and to formulate a self-calibration pipeline [10].

Authors of [15] address the deployment and self-calibration challenge of an all-in-one CDPR equipped with

[1]https://github.com/MohammadrezaDindarloo/ARASFactorSLAC.

an onboard inclinometer. This work considers the cable sag in the calibration process but does not verify large-scale robots and does not leverage factor-graphs to formulate the problem. Our work is closely related to [10] in terms of problem formulation and to [15], [16] in terms of cable modeling. In this study, we advance our graph-based calibration approach previously introduced in [10] to encompass large-scale applications involving sagging cables. Moreover, we conduct finite element simulation studies to validate our model and calibration pipeline for large-scale robots. Furthermore, we present comparative analyses that highlight the importance of precise cable sag modeling.

III. PRELIMINARIES

A. Notations and Definitions

This paper considers a suspended CDPR with six DoFs ($m = 6$) and four actuated cables ($n = 4$). Since $m > n$, this robot is underactuated and forms an under-constrained structure [17]. Fig. 1 depicts the structure of this robot, highlighting only one cable for the sake of simplicity. The frame $\mathcal{L}$ is attached to the moving platform of the robot, while the global frame $\mathcal{G}$ is attached to the base. The pose of the end effector with respect to the global frame is represented by $(\boldsymbol{p}, \boldsymbol{R}) \in \mathrm{SE}(3)$, where $\boldsymbol{p} \in \mathbb{R}^3$ is the translation vector from $\mathcal{G}$ to $\mathcal{L}$, and $\boldsymbol{R} \in \mathrm{SO}(3)$ is the orientation of $\mathcal{L}$ with respect to $\mathcal{G}$. Cable i leaves the base at point $\boldsymbol{p}_{a_i}$ defined in the global frame and connects to the end-effector at point $\boldsymbol{p}_{b_i}$ expressed in the local body frame.

We model the cable sag within a vertical 2D plane Ψ that contains pulley $\boldsymbol{p}_{a_i}$ and the attachment point $\boldsymbol{p}_{b_i}$. Frame $\mathcal{P}$ on this plane is originated at $\boldsymbol{p}_{a_i}$ and is defined by unit vectors $\hat{\boldsymbol{s}}_z$ parallel to the global z axis, and $\hat{\boldsymbol{s}}_c$ along the cable direction projected onto the $x_{\mathcal{P}} - y_{\mathcal{P}}$ plane of the $\mathcal{P}$ frame. Specifically, $\hat{\boldsymbol{s}}_c = \frac{\boldsymbol{b}_{xy_i} - \boldsymbol{a}_{xy_i}}{\|\boldsymbol{b}_{xy_i} - \boldsymbol{a}_{xy_i}\|}$, where $\boldsymbol{b}_{xy_i}$ and $\boldsymbol{a}_{xy_i}$ are the $x-y$ components of $\boldsymbol{b}_i$ and $\boldsymbol{a}_i$ in the global frame.

B. The Catenary Equations

Catenary equations describe the sagging effect in an inextensible cable with non-negligible mass as described by [18]:

$$z_i(x_c) = \frac{f_{h,i}}{g_c} \cdot \left(\cosh\left(\frac{g_c}{f_{h,i}} \cdot (x_c + C_{1,i}) \right) - C_{2,i} \right) \tag{1}$$

In this equation, the cable's sagging shape is defined by the function $z_i(x_c)$. The catenary constants, $C_{1,i}$ and $C_{2,i}$ are determined by the endpoint boundary conditions $z_i(0) = (\boldsymbol{p}_a)_z$ and $z_i'(L_i) = -\frac{f_v}{f_h}$, where $z_i'(L_i)$ is the slope of Eq.(1) at $x_c = L_i = \|(\boldsymbol{b})_{xy_i} - (\boldsymbol{a})_{xy_i}\|$ and have the following closed-form solution:

$$C_{1,i} = \frac{f_{h,i}}{g_c} \cdot \operatorname{asinh}\left(\frac{-f_{v,i}}{f_{h,i}} \right) - L_i \tag{2}$$

$$C_{2,i} = \cosh\left(C_{1,i} \cdot \frac{g_c}{f_{h,i}} \right) - \frac{g_c}{f_{h,i}} \cdot (\boldsymbol{p}_a)_z \tag{3}$$

As shown in Fig. 1, $f_{h,i}$ and $f_{v,i}$ are the horizontal and vertical components of the cable force $\mathbf{f}_{c_i}$ expressed in frame $\mathcal{P}$. Furthermore, $g_c = g.\rho_c$ where g and ρ_c are the gravitational acceleration and the mass per unit cable length, respectively. Finally, the curve length of Eq.(1) is defined as the true cable length $l_{C,i}$ and is computed as follows:

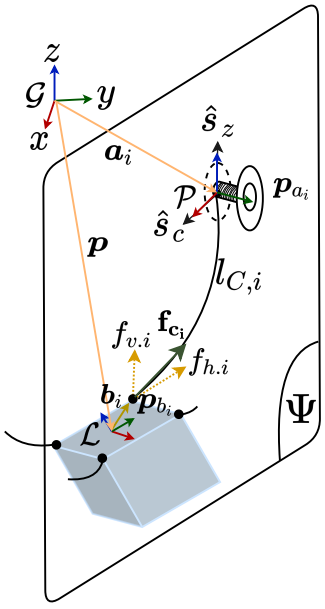

Fig. 1. End-effector diagram

$$\begin{aligned} l_{C,i} &= \int_0^{L_i} \sqrt{1 + \left(\frac{dz}{dx}\right)^2}\, dx \\ &= \frac{f_{h,i}}{g_c} \cdot \left(\sinh\left(\frac{g_c}{f_{h,i}} (L_i + C_{1,i}) \right) - \sinh\left(\frac{g_c}{f_{h,i}} \cdot C_{1,i} \right) \right) \end{aligned} \tag{4}$$

C. The Kinematics of the Robot

The study of kinematics in an underactuated Cable-Driven Parallel Robot (CDPR) encompasses its geometric properties along with its static equations, commonly referred to as kineto-static analysis [19]. End-effector wrench $\mathbf{w}_{ee} \in \mathbb{R}^6$ is mapped into the cable forces $\mathbf{f}_c \in \mathbb{R}^4$ through the Jacobian matrix $\boldsymbol{J} \in \mathbb{R}^{4\times 6}$:

$$\mathbf{w}_{ee} = \boldsymbol{J}^T \mathbf{f}_c \tag{5}$$

In this paper, we assume that $\mathbf{w}_{ee}$ is induced only by gravity, and it is computed as follows:

$$\mathbf{w}_{ee} = \begin{bmatrix} \hat{\boldsymbol{s}}_z \\ \boldsymbol{b}_{\mathrm{com}} \times \hat{\boldsymbol{s}}_z \end{bmatrix} m_e g \tag{6}$$

where m_e is the end-effector mass and $\boldsymbol{b}_{com}$ is offset between the origin of $\mathcal{L}$ and the end-effector's center of mass (CoM). To couple these statics equations to the catenary model in Eq. (4), each cable tension component is represented as a tuple of horizontal and vertical parts:

$$\mathbf{f}_{c_i} = \begin{bmatrix} f_{h,i} & f_{v,i} \end{bmatrix}^T \tag{7}$$

For each $\mathbf{f}_{c_i}$, the corresponding i^{th} column of the Jacobian

matrix $\boldsymbol{J}^T$ is expressed as:

$$\boldsymbol{J}_i^T = \begin{bmatrix} -\hat{\boldsymbol{s}}_{c,i} & \hat{\boldsymbol{s}}_z \\ -\boldsymbol{R}\boldsymbol{b}_i \times \hat{\boldsymbol{s}}_{c,i} & \boldsymbol{R}\boldsymbol{b}_i \times \hat{\boldsymbol{s}}_z \end{bmatrix} \tag{8}$$

where the rotation matrix $\boldsymbol{R}$, unit vectors $\hat{\boldsymbol{s}}_{c,i}, \hat{\boldsymbol{s}}_z$, and the end-effector attachment vector $\boldsymbol{b}_i$ in the local frame, are defined in Sec. III-A. Note that the statics relation in Eq. (5) describes an underdetermined problem where the number of equations is less than the number of variables. As suggested in [16], we express all the cable forces based on one reference cable. As it will be seen in Sec. IV, this selection reduces the required number of force sensors to only one. As presented in [6], [16], by partitioning the Jacobian matrix and the force vector, one may write Eq. (5) as:

$$\mathbf{w}_{ee} = \begin{bmatrix} \boldsymbol{J}_{\text{ref}}^T & \boldsymbol{J}_{\text{res}}^T \end{bmatrix} \cdot \begin{bmatrix} \mathbf{f}_{c_{\text{ref}}} \\ \mathbf{f}_{c_{\text{res}}} \end{bmatrix} \tag{9}$$

$$= \boldsymbol{J}_{\text{ref}}^T \cdot \mathbf{f}_{c_{\text{ref}}} + \boldsymbol{J}_{\text{res}}^T \cdot \mathbf{f}_{c_{\text{res}}} \tag{10}$$

where $\boldsymbol{J}_{\text{ref}}^T$ denotes a 6×2 sub-matrix containing the first two columns of $\boldsymbol{J}^T$ that correspond to the reference cable force $\mathbf{f}_{c_{\text{ref}}}$. Subsequently, $\boldsymbol{J}_{\text{res}}^T$ is defined as the remaining 6×6 sub-matrix, and $\mathbf{f}_{c_{\text{res}}}$ represents the remaining cable forces. We can solve for $\mathbf{f}_{c_{\text{res}}}$ in Eq. (10) as follows:

$$\mathbf{f}_{c_{\text{res}}} = (\boldsymbol{J}_{\text{res}}^T)^{-1} \left(\mathbf{w}_{ee} - \boldsymbol{J}_{\text{ref}}^T \cdot \mathbf{f}_{c_{\text{ref}}} \right) \tag{11}$$

By adopting this formulation, the number of variables is reduced from 8 to 2, while the statics equality is implicitly encoded in Equation (5), eliminating the necessity for a constrained solver [6].

IV. Graph-Based Kineto-Static Calibration

This section presents a graphical energy model to represent the kineto-static model of the robot. The variables in this energy model correspond to the kinematic parameters of interest, which are interconnected through the sensory measurements and equations outlined in Section III.

A. Problem Definition

The kinematic calibration problem can be formulated as the following nonlinear programming problem:

$$\begin{aligned} &\min_{\boldsymbol{\theta}} \sum_{i=1}^{N} f(\boldsymbol{\theta}, \mathbf{z}_i) \\ &\text{s.t. } \mathbf{C}(\boldsymbol{\theta}) \geq \mathbf{0} \end{aligned} \tag{12}$$

In this formulation, $\boldsymbol{\theta}$ represents the parameters of interest, $\mathbf{C}(\boldsymbol{\theta}) \geq \mathbf{0}$ denotes constraints on these parameters, and $f(\boldsymbol{\theta}, \mathbf{z}_i)$ serves as an energy function that assigns high values to parameters that fail to adequately explain the data samples $\mathbf{z}_i$ (i.e., sensory measurements).

In this paper, $\boldsymbol{\theta}$ encompasses the pulley locations on the base and the unknown cable length offsets for the relative cable length encoders. The sample points $\mathbf{z}_i$ are the relative cable length measurements, end-effector poses estimated by an onboard localization system (e.g. visual SLAM pipeline), and the tension force of one of the cables (i.e. reference cable) measured at the end-effector using a load-cell sensor. Furthermore, this paper incorporates the constraints into the $f(\cdot)$ function as penalty terms.

During the calibration procedure, we assume that the end-effector can be moved to stationary locations within the workspace while being supported by the cables to allow for reading the sensors at equilibrium configuration. Empirically, it is essential for these sample points to encompass a broad spectrum of translational degrees of freedom.

B. Factor Graph Representation

The nonlinear programming formulation defined in Eq. (12) may be expressed as a graphical model comprised of nodes that represent the decision variables and edges that encode constraints between them as functions of sensory measurements. In the robotics community, factor graphs are one example of such representation [20]. They offer a robust and adaptable framework for articulating diverse problems, spanning from state estimation to motion planning, and reveal the sparsity structure of the problem, facilitating the utilization of highly efficient solvers.

Formally, one may use the bipartite graphs $F = (\mathcal{U}, \mathcal{V}, \mathcal{E})$, where factors ($\Phi_i \in \mathcal{U}$), in which variables ($x \in \mathcal{V}$) act as nodes, and their relations are represented by edges ($e_{ij} \in \mathcal{E}$). The set of variables connected to factor Φ_i is denoted as $\boldsymbol{\zeta}_i$. Essentially, a factor graph (F) reveals how the energy function $\Phi(\boldsymbol{\zeta})$ is factorized:

$$\Phi(\boldsymbol{\zeta}) = \prod_i \Phi_i(\boldsymbol{\zeta}_i) \tag{13}$$

Minimizing the logarithm of the likelihood function $\Phi(\boldsymbol{\zeta})$ leads to a nonlinear program that defines the problem at hand. In the following sections, we describe the kineto-static and constraint factors necessary to clarify our calibration issue, along with its associated factor-graph representation.

C. Kineto-Static Self-Calibration Factor Graph

Our approach defines a factor graph with variable nodes $\boldsymbol{X}(k) \in \text{SE}(3)$, l_i^0, $\boldsymbol{p}_{a_i} \in \mathbb{R}^3$, $\Delta\mathcal{R}(k) \in \text{SO}(3)$, and $f_h^{ref}(k)$, $f_v^{ref}(k) \in \mathbb{R}$. These nodes represent the end-effector poses, cable length measurement offsets, anchor point locations, and changes in robot orientation, as well as the reference cable force in the horizontal and vertical axes in static poses, respectively. In our underactuated configuration, not all of the combinations of position and orientation are feasible. Here, $\Delta\mathcal{R}(k)$ is a variable that modifies the initial value of the end-effector rotation. Furthermore, the reference cable is designated as the cable for which the user installs a force sensor for calibration purposes.

Fig. 2 illustrates the structure of this self-calibration factor graph visualized for two static pose samples 0 and i. Optimization variables in this graph are represented by labeled circles with distinct colors. Moreover, the factors are depicted by colored squares, with the encoder factor illustrated in yellow, the cable attachment factor in red, the force measurement factor in green, and the pose prior factor in blue.

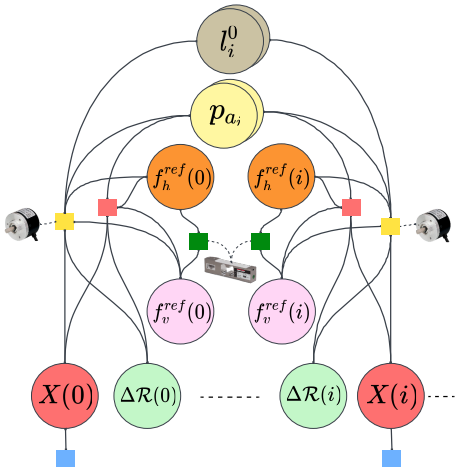

Fig. 2. Kinematic calibration factor graph

Each factor is derived based on the kinematic and catenary equations described in Sec. III and are as follows:

1) Catenary Length Factor: This factor imposes a relationship between the encoder measurements and the catenary length. This measurement constraint for the i^{th} cable can be formulated as:

$$f(z_i^{enc}, \boldsymbol{\zeta})[k] = l_{C,i}[k] + l_i^0 - z_i^{enc}[k] \tag{14}$$

where $l_{C,i}$ represents the cable sag length as defined in Eq. 4, l_i^0 denotes the cable length offset, and z_i^{enc} represents the relative encoder measurement corresponding to the i^{th} cable. Additionally, k represents the data time sample index.

2) Cable Attachment Factor: This factor guarantees consistency between the computed height of the cable attachment point on the end-effector, deduced from the end-effector pose, and the anticipated catenary height originating from the corresponding pulley. The error function for the i^{th} anchor can be expressed as:

$$f(\boldsymbol{\zeta})[k] = (p_{b,i})_z[k] - z_i(L_i)[k] \tag{15}$$

where, $(p_{b,i})_z$ refers to the height of the i^{th} cable attachment point in the global frame, and $z_i(L_i)$ represents the cable's sagging shape at L_i as described in Eq. 1.

3) Force Measurement Factor: This factor constrains the norm of the horizontal and vertical forces to be close to the force measurement from a cable tension load cell on the end-effector. Note that this constraint is needed only for the reference cable with a penalty term expressed as:

$$f(f^m, \boldsymbol{\zeta})[k] = \|[f_h^{ref}[k] \quad f_v^{ref}[k]]^T\| - f^m[k] \tag{16}$$

Here, f_h^{ref} and f_v^{ref} represent the reference cable forces in the horizontal and vertical directions, respectively, $\|.\|$ denotes the Euclidean norm, and f^m is the value of reference cable tension measured by the force sensor.

4) Pose Prior Factor: The encoder and force measurement factors are associated with pose variable nodes $\boldsymbol{X}(k)$, representing the robot's static poses in the calibration procedure as measured by an onboard vision-based localization system. Each pose corresponds to equilibrium states wherein the robot is stationary via its four cables. Instances of static poses in Fig. 2 are labeled with markers 0 and i

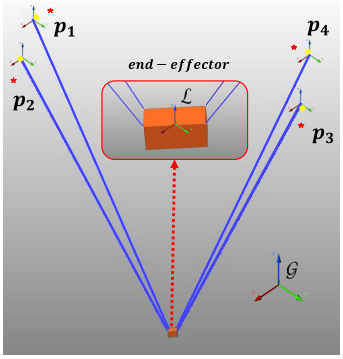

Fig. 3. Small-scale robot scenario in the RecurDyn simulator environment

V. Simulation Results

This section aims to validate the proposed model and calibration procedure through a FE simulation of the system. First, the validity of the kineto-static formulations is investigated, and then the calibration results for two representative small and large-scale cable robots are demonstrated. We have used the RecurDyn software [21] for FE simulations, implemented our factor graph using the GTSAM library [22], and employed SymForce [23] to derive our factors and corresponding Jacobians.

A. Model Verification

To verify the accuracy of our kineto-static model, as described in Section III, we constrained the kineto-static calibration factor graph, which is outlined in Section IV, with prior factors on variables extracted from the simulator. We set up two scenarios of a small and a large-scale suspended cable-driven robot. Fig. 3 and Fig. 4 show these robots scenarios in the RecurDyn simulator environment, respectively. Both robots have four cables attached to the upper four corners of a rectangular cuboid with dimensions of $(12.5, 4.5, 28.5)$ meters for the small robot and $(240, 220, 50)$ meters for the large one, as mentioned in Table I. The end-effector mass for the large robot is set to $34Kg$ and for the smaller robot, it is set to $4.4Kg$. The cable's length density for the small robots is $10.2g/m$ and for the larger robot, it is $72.4g/m$, which translates into a relative end-effector to cable mass ratio of 4.14 for the small robot and 0.62 for the

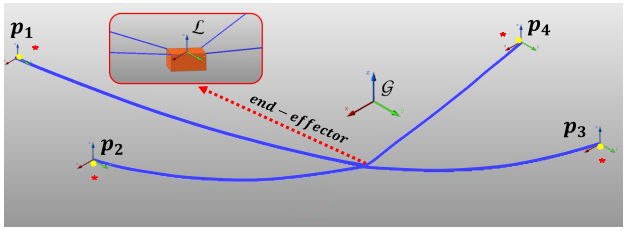

Fig. 4. Large-scale robot scenario in the RecurDyn simulator environment

TABLE I
MODEL VERIFICATION

Scenario	Large scale	Small scale
MPE-L (%)	8.8947×10^{-3}	7.3595×10^{-3}
MPE-F (%)	0.9154	0.9046
$[l_{\min}, l_{\max}]$ (m)	[134.7, 200.7]	[10.8, 25.9]
$[f_{\min}, f_{\max}]$ (N)	[489.1, 954.3]	[12.4, 26.2]
Pulley configuration (m^3)	$240 \times 220 \times 50$	$12.5 \times 4.5 \times 28.5$
End-effector mass (Kg)	34.0	4.4
Cable properties	ρ = 1.44 (g/cm^2) radius = 4.0 (mm)	ρ = 1.44 (g/cm^2) radius = 1.5 (mm)

larger one. As suggested in [18], these conditions imply a notable sagging effect for the larger robot.

The first two rows of Table I present the mean percentage errors in predicted cable length (MPE-L) and force (MPE-F) computed over 5 random static poses. These values indicate a close match between the cable force and catenary cable length values calculated from our mathematical model and the corresponding values from the simulator. Specifically, for the large-scale robot, MPE-L, and MPE-F are evaluated to be %0.0089 and %0.9154, respectively, which are very small compared to the cable length and force ranges for each robot, as also provided in the table. As intuitively expected, this match is more precise for the small-scale cable robot, whose predicted cable length and forces are indicated in the third column of this table.

B. Calibration

In this section, we implement the calibration procedure proposed in this paper as outlined in Section IV and highlight the significance of modeling cable sag through the simulation results. Additionally, we briefly address the calibration initialization issue and suggest a potential solution.

Our aim in the kinematic calibration process is to determine the anchor point locations and cable length encoder offsets by utilizing measurements of a set of end-effector poses, relative cable-length measurements, and only the tension values of the reference cable at the end-effector attachment point. According to our experiments, it is crucial for the sample distribution to comprehensively cover the pose range of the robot. The development of analytical and observation-aware trajectory generation for addressing this identification problem is a subject for future research.

We obtained our simulated sensor data from the RecurDyn software and introduced zero-mean Gaussian noise perturbations to incorporate the anticipated sensor noise. In particular, we applied a standard deviation of $10mm$ for cable length, $5N$ for the force sensor of the large-scale robot, and $1N$ for that of the small robot. The end-effector poses were perturbed by $\Delta\mathbf{T} = \exp(\hat{\boldsymbol{\xi}})$ where $\hat{\boldsymbol{\xi}} \in \mathfrak{se}(3)$ represents a Lie algebra element corresponding to a twist vector $\boldsymbol{\xi} \in \mathbb{R}^6$. These perturbation twist vectors are sampled from a zero-mean Gaussian distribution $\boldsymbol{\xi} \sim \mathcal{N}(\mathbf{0}, \boldsymbol{\Sigma})$ with covariance matrix $\boldsymbol{\Sigma}$ chosen to have a deviation of 0.005 meters in the translation and 0.01 radians in rotational degrees of freedom. To initialize the factor-graph, we perturbed the ground-truth anchor-point locations with a magnitude of 1 meter for the small robot and 10 meters for the large platform. Furthermore, these perturbations for the initial cable offsets were set as 10 meters and 80 meters for the small and large robots, respectively. We considered the initial guess for the reference cable force in the vertical axis as $f_{v_0}^{ref} = m_e g/4$, and for the horizontal axis as:

$$f_{h_0}^{ref} = \frac{f_{v_0}^{ref}}{\tan(\alpha)} \tag{17}$$

where α is defined as:

$$\alpha = \cos^{-1}\left(\frac{\hat{\boldsymbol{s}}_{c_{ref}}^T \cdot [\boldsymbol{p}_{b_{\text{ref}}} - \boldsymbol{p}_{a_{\text{ref}}}]}{\|\boldsymbol{p}_{b_{\text{ref}}} - \boldsymbol{p}_{a_{\text{ref}}}\|}\right) \tag{18}$$

In this context, $\hat{\boldsymbol{s}}_{c_{ref}}$ denotes the unit vector as defined in Sec.III, utilizing the initial estimates for the pulley position. It is important to note that these points correspond to the anchors associated with the reference cable.

TABLE II
CALIBRATION RESULTS WITH PROPOSED ALGORITHM

Scenario / MAE (m)	large (9 poses)	large (18 poses)	large (35 poses)	short (8 poses)
$\text{Pulley}_{\text{Avg.}}$	0.387	0.226	0.191	0.149
$\text{Offset}_{\text{Avg.}}$	0.380	0.217	0.173	0.115

The calibration results for anchor locations and cable length offsets are given in Table II. These results correspond to the scenarios depicted in Fig.3 and Fig.4, where the initial anchor locations are denoted by red stars, while the calibrated anchor locations are indicated by yellow circles for both cases. In this Table, three different calibration scenarios are reported for the large-scale robot with different numbers of sample points used for the optimization routine. As expected, the calibration accuracy improves with more sample points and yields more accurate results with 35 data samples for the large robot and 8 sample poses for the small one. We believe that for the larger robot, the parameters corresponding to the cable sag have a more profound impact on the calibration accuracy. This in turn increases the effective number of model parameters and requires more sample points for proper identification.

VI. DISCUSSIONS

A. Importance of Considering Cable Sag

To investigate the significance of considering the cable sag effect, we conduct the calibration procedure for the larger robot using a simplified factor-graph that utilizes a massless rigid cable model, as reported in [10]. Consequently, due to this simplification, the mean absolute error significantly deteriorates from 0.19 to 2.34 meters, indicating a substantial decrease in calibration accuracy. This significant disparity

in calibration quality emphasizes the crucial importance of accounting for cable sag.

B. Notes on The Initialization Procedure

As indicated in [10], a major concern in solving a non-convex and non-linear calibration optimization problem is its proper initialization. If the initial values are not close enough to the global solution, the result may be highly skewed or the optimizer may even diverge. The framework presented in [10] attempts to solve this initialization issue by warm-starting the nonlinear least square optimizer with the rough output of a global Monte Carlo optimization algorithm. However, [10] assumes a rigid cable model with no sagging effects.

We believe that this algorithm may directly be employed to initialize the extended calibration problem presented in this paper. As mentioned earlier, the calibration accuracy of the large cable robot with a simplified cable model was 2.34 meters. This value is considerably smaller than the perturbations we applied during our calibration experiments (10 meters). This indicates that we can safely initialize our optimization algorithm with the outputs of a similar algorithm as presented in [10]. The validation of this hypothesis for the specific cases presented in this paper was not possible due to the limitations of the employed simulator for generating images/LiDAR sensor data required for running this algorithm. Investigation of this idea using photo-realistic simulators is the subject of future research.

VII. Conclusions

This paper proposed a self-calibration framework for cable robots with cable sagging effect. We formulated the kineto-static calibration problem using a unified factor-graph representation and validated its feasibility and accuracy of our model using a finite element analysis software for two representative small and large-scale cable robots. Specifically, we showed significant accuracy improvement from 2.34 meters to 0.19 meters. The proposed graph-based framework in this paper may directly be used to localize the end-effector after calibration. Specifically, the results of the calibration may be incorporated as prior factors on the kinematic parameters while the end-effector pose is treated as unknown. We aim to explore this idea and also the possibility of adding other sensory modaliteis in the future.

References

[1] G. Chen, S. Baek, J.-D. Florez, W. Qian, S.-w. Leigh, S. Hutchinson, and F. Dellaert, "Gtgraffiti: Spray painting graffiti art from human painting motions with a cable driven parallel robot," in *2022 International Conference on Robotics and Automation (ICRA)*. IEEE, 2022, pp. 4065–4072.

[2] F. Takemura, K. Maeda, and S. Tadokoro, "Attitude stability of a cable driven balloon robot," in *2006 IEEE/RSJ International Conference on Intelligent Robots and Systems*. IEEE, 2006, pp. 3504–3509.

[3] P. Miermeister, M. Lächele, R. Boss, C. Masone, C. Schenk, J. Tesch, M. Kerger, H. Teufel, A. Pott, and H. H. Bülthoff, "The cablerobot simulator large scale motion platform based on cable robot technology," in *2016 IEEE/RSJ International Conference on Intelligent Robots and Systems (IROS)*. IEEE, 2016, pp. 3024–3029.

[4] A. Riechel, P. Bosscher, H. Lipkin, and I. Ebert-Uphoff, "Cable-driven robots for use in hazardous environments," in *Proceedings of 10th International Conference on Robotics and Remote systems for Hazardeous Enviromnments, Gainesville*, 2004.

[5] B. Zhang, F. Zhou, W. Shang, and S. Cong, "Auto-calibration and online-adjustment of the kinematic uncertainties for redundantly actuated cable-driven parallel robots," in *2019 IEEE 4th International Conference on Advanced Robotics and Mechatronics (ICARM)*. IEEE, 2019, pp. 280–285.

[6] P. H. Borgstrom, B. L. Jordan, B. J. Borgstrom, M. J. Stealey, G. S. Sukhatme, M. A. Batalin, and W. J. Kaiser, "Nims-pl: A cable-driven robot with self-calibration capabilities," *IEEE Transactions on Robotics*, vol. 25, no. 5, pp. 1005–1015, 2009.

[7] E. Idá, J.-P. Merlet, and M. Carricato, "Automatic self-calibration of suspended under-actuated cable-driven parallel robot using incremental measurements," in *Cable-Driven Parallel Robots: Proceedings of the 4th International Conference on Cable-Driven Parallel Robots 4*. Springer, 2019, pp. 333–344.

[8] A. Pott and T. Bruckmann, *Cable-driven parallel robots*. Springer, 2013.

[9] D. Lau, "Initial length and pose calibration for cable-driven parallel robots with relative length feedback," in *Cable-Driven Parallel Robots: Proceedings of the Third International Conference on Cable-Driven Parallel Robots*. Springer, 2018, pp. 140–151.

[10] R. Khorrambakht, H. Damirchi, M. Dindarloo, A. Saki, S. Khalilpour, H. D. Taghirad, and S. Weiss, "Graph-based visual-kinematic fusion and monte carlo initialization for fast-deployable cable-driven robots," in *2023 IEEE/RSJ International Conference on Intelligent Robots and Systems (IROS)*. IEEE, 2023, pp. 1832–1839.

[11] N. Tremblay, K. Kamali, P. Cardou, C. Desrosiers, M. Gouttefarde, and M. J.-D. Otis, "Eye-on-hand calibration method for cable-driven parallel robots," in *Cable-Driven Parallel Robots: Proceedings of the 4th International Conference on Cable-Driven Parallel Robots 4*. Springer, 2019, pp. 345–356.

[12] R. Khorrambakht, H. Damirchi, S. Khalilpour, and H. Taghirad, "A calibration framework for deployable cable driven parallel robots with flexible cables," in *2019 7th International Conference on Robotics and Mechatronics (ICRoM)*. IEEE, 2019, pp. 552–557.

[13] H. Bayani, M. T. Masouleh, and A. Kalhor, "An experimental study on the vision-based control and identification of planar cable-driven parallel robots," *Robotics and Autonomous Systems*, vol. 75, pp. 187–202, 2016.

[14] G. Chen, S. Hutchinson, and F. Dellaert, "Locally optimal estimation and control of cable driven parallel robots using time varying linear quadratic gaussian control," in *2022 IEEE/RSJ International Conference on Intelligent Robots and Systems (IROS)*. IEEE, 2022, pp. 7367–7374.

[15] H. An, H. Liu, X. Liu, and H. Yuan, "An all-in-one cable-driven parallel robot with flexible workspace and its auto-calibration method," in *2022 IEEE/RSJ International Conference on Intelligent Robots and Systems (IROS)*. IEEE, 2022, pp. 7345–7351.

[16] E. Allak, R. Khorrambakht, C. Brommer, and S. Weiss, "Kinematics-inertial fusion for localization of a 4-cable underactuated suspended robot considering cable sag," in *2022 IEEE/RSJ International Conference on Intelligent Robots and Systems (IROS)*. IEEE, 2022, pp. 4989–4996.

[17] E. Idà, S. Briot, and M. Carricato, "Natural oscillations of underactuated cable-driven parallel robots," *IEEE Access*, vol. 9, pp. 71 660–71 672, 2021.

[18] A. Pott and T. Bruckmann, *Cable-driven parallel robots*. Springer, 2013.

[19] M. Carricato, "Direct geometrico-static problem of underconstrained cable-driven parallel robots with three cables," *Journal of Mechanisms and Robotics*, vol. 5, no. 3, p. 031008, 2013.

[20] F. Dellaert, "Factor graphs: Exploiting structure in robotics," *Annual Review of Control, Robotics, and Autonomous Systems*, vol. 4, pp. 141–166, 2021.

[21] FunctionBay, Inc., "Recurdyn: Multi-body dynamics cae software," https://functionbay.com/en/page/single/2/recurdyn-overview, 2023.

[22] F. Dellaert, "Factor graphs and gtsam: A hands-on introduction," *Georgia Institute of Technology, Tech. Rep*, vol. 2, p. 4, 2012.

[23] H. Martiros, A. Miller, N. Bucki, B. Solliday, R. Kennedy, J. Zhu, T. Dang, D. Pattison, H. Zheng, T. Tomic, P. Henry, G. Cross, J. VanderMey, A. Sun, S. Wang, and K. Holtz, "SymForce: Symbolic Computation and Code Generation for Robotics," in *Proceedings of Robotics: Science and Systems*, 2022.